Regularized selection indices for breeding value prediction using hyper-spectral image data

by

Marco Lopez-Cruz[1], Eric Olson[1], Gabriel Rovere[2,3,4], Jose Crossa[6], Susanne Dreisigacker[6], Suchismita Mondal[6], Ravi Singh[6], and Gustavo de los Campos[3,4,5,*]

[1]Department of Plant, Soil and Microbial Sciences, Michigan State University, USA

[2]Department of Animal Science, Michigan State University, USA

[3]Department of Epidemiology and Biostatistics, Michigan State University, USA

[4]Institute for Quantitative Health Science and Engineering, Michigan State University, USA

[5]Department of Statistics and Probability, Michigan State University, USA

[6]International Maize and Wheat Improvement Center (CIMMYT), Mexico

*Correspondence and request should be addressed to G.D.L.C. (e-mail: gustavoc@msu.edu).

Abstract

High-throughput phenotyping (HTP) technologies can produce data on thousands of phenotypes per unit being monitored. These data can be used to breed for economically and environmentally relevant traits (e.g., drought tolerance); however, incorporating high-dimensional phenotypes in genetic analyses and in breeding schemes poses important statistical and computational challenges. To address this problem, we developed regularized selection indices; the methodology integrates techniques commonly used in high-dimensional phenotypic regressions (including penalization and rank-reduction approaches) into the selection index (SI) framework. Using extensive data from CIMMYT's (International Maize and Wheat Improvement Center) wheat breeding program we show that regularized SIs derived from hyper-spectral data offer consistently higher accuracy for grain yield than those achieved by canonical SIs, and by vegetation indices commonly used to predict agronomic traits. Regularized SIs offer an effective approach to leverage HTP data that is routinely generated in agriculture; the methodology can also be used to conduct genetic studies using high-dimensional phenotypes that are often collected in humans and model organisms including body images and whole-genome gene expression profiles.

Introduction

High-throughput phenotyping (HTP) technologies have been adopted at a fast pace in agriculture; applications range from the use of HTP in highly controlled environments (e.g., growth chambers[1]) to extensive HTP using sensing devices mounted on aerial (e.g., hyper-spectral

cameras mounted on aerial vehicles[2]) and terrestrial equipment such as tractors and combine harvesters[3]. Modern agricultural production systems use HTP data to optimize management practices[4], forecast agricultural outputs[5] and to assess the quality (e.g., protein content) of agricultural commodities[6]. HTP data can also be a valuable input for breeding programs. For instance, extensive HTP may enable an expansion of genetic testing that can lead to higher intensity of selection and faster genetic progress. Moreover, HTP data may offer opportunities to improve traits such as drought tolerance that are otherwise difficult to measure and breed for.

Sensors can generate data on hundreds or thousands of phenotypes per unit being monitored. For example, hyper-spectral cameras can generate reflectance of electromagnetic power at hundreds of wavelengths in the visible and infrared spectrum. These measurements can be considered as indicator phenotypes that can be used to predict other traits. An extensive body of research deals with the use HTP data to predict phenotypes such as grain yield[5,7–9], dry matter[3], oil and protein content[10,11]. However, there has been much less research on how to integrate HTP data in genetic studies and in breeding schemes. In genetics, the problem of predicting the genetic merit of a target trait given a set of correlated phenotypes was first addressed by Smith[12] and Hazel[13] who introduced the concept of selection index (SI) in plant and animal breeding, respectively.

A SI seeks to improve a target trait y_i (e.g., grain yield) using information from another set of measured traits (e.g., hyper-spectral image data). A linear SI is a weighted sum of the measured phenotypes with weights derived to maximize the correlation between the genetic merit for the selection target and the SI. Thus, the SI methodology offers a natural framework for integrating HTP data into breeding decisions. However, when the measured phenotype is high-

62 dimensional, the naïve application of the SI can lead to overfitting and sub-optimal accuracy of
63 indirect selection.

64 To address this problem, we developed regularized selection indices (including penalized
65 and reduced-rank methods) that are tailored to achieve accurate prediction of genetic values
66 using high-dimensional phenotypes. The proposed methodology integrates into the SI framework
67 methods often used to prevent overfitting in high-dimensional phenotypic regressions[14]. Using
68 extensive multi-environment crop imaging data from CIMMYT's wheat breeding program we
69 show that regularized SIs offer improved accuracy of indirect selection in both optimal and stress
70 environments.

71

72 # Results

73 A **selection index** is a linear combination of p measured phenotypes, $\boldsymbol{x}_i = (x_{i1}, \dots, x_{ip})'$, of the
74 form $I_i = \boldsymbol{x}_i'\boldsymbol{\beta}$, where $\boldsymbol{\beta} = (\beta_1, \dots, \beta_p)'$ is a vector of regression coefficients whose entries define
75 the weights of each of the measured phenotypes in the SI. In a canonical SI those weights are
76 derived by minimizing the expected squared deviation between the genetic merit for the
77 selection goal (g_{y_i}, e.g., the genetic merit for grain yield of the ith genotype) and the index, that
78 is:

79 $$\widehat{\boldsymbol{\beta}} = \arg\min_{\beta} \frac{1}{2} \mathbb{E}\left(g_{y_i} - \boldsymbol{x}_i'\boldsymbol{\beta}\right)^2. \quad (1)$$

80 The solution to this optimization problem is (see *Methods* section):

81 $$\widehat{\boldsymbol{\beta}} = \boldsymbol{P}_x^{-1}\boldsymbol{G}_{x,y}, \quad (2)$$

82 where $\boldsymbol{G}_{x,y} = \mathbb{E}(\boldsymbol{x}_i g_{y_i}) = \left(G_{x_1,y}, \dots, G_{x_p,y}\right)'$ is a vector containing the genetic covariances

83 between the selection objective (y_i) and each of the measured traits ($\boldsymbol{x}_i$), and $\boldsymbol{P}_x$ is the

84 (population) phenotypic variance-covariance matrix of the measured phenotypes, that is, $\boldsymbol{P}_x =$

85 $\mathbb{E}(\boldsymbol{x}_i\, \boldsymbol{x}_i') = \mathrm{Cov}(\boldsymbol{x}_i, \boldsymbol{x}_i')$. Thus, a canonical SI takes the form $I_i = \boldsymbol{x}_i' \boldsymbol{P}_x^{-1} \boldsymbol{G}_{x,y}$. The theory

86 underlying the derivation of SIs and response to indirect selection is well established[15,16].

87 The SI is by construction the best linear predictor (BLP) of the genetic merit for the

88 selection goal; this property holds when $\boldsymbol{G}_{x,y}$ and $\boldsymbol{P}_x$ are known. However, when the number of

89 measured phenotypes is large, errors in the estimation of $\boldsymbol{P}_x$ and $\boldsymbol{G}_{x,y}$ may lead to overfitting

90 and sub-optimal accuracy of indirect selection.

91 **Regularized selection indices**

92 Reduced-rank (e.g., principal components methods) and penalized regression[14] are two

93 approaches commonly used to confront overfitting in high-dimensional regression problems.

94 These methodologies were developed for regression problems involving an observable

95 phenotype (y_i). In the SI, the response (g_{y_i}) is unobservable; however, the same principles that

96 are applied in phenotypic reduced-rank and penalized regressions can be integrated into the SI

97 framework.

98 **Reduced-rank selection indices**. In principal components (PC) regression, the response is

99 regressed on a reduced number ($q < p$) of PCs extracted from a set of predictors ($\boldsymbol{x}_i$); the same

100 concept can be used to derive a reduced-rank SI. For instance, one can extract a reduced number

101 of PCs from a crop image and the resulting PCs can be used as 'measured traits' in equation (1).

The solution of equation (1) will render estimates of the regression coefficients for the PCs, which can be transformed back to coefficients applicable to the measured traits (see *Methods*). Thus, a reduced-rank SI (referred to as PC-SI) can be derived following these steps: (*i*) extract, using the singular value decomposition, q PCs from the matrix containing the measured phenotypes, (*ii*) estimate the genetic covariances between the first q PCs and the selection objective, (*iii*) use these estimated (co)variances to derive coefficients associated with the top q PCs; finally, (*iv*) transform these coefficients into coefficients for the measured phenotypes. This process can be done using $q = 1,2,\dots,p$ PCs ($q = p$ renders the canonical SI). For the sequence of estimates $(\widehat{\boldsymbol{\beta}}^{(1)}, \widehat{\boldsymbol{\beta}}^{(2)}, \dots, \widehat{\boldsymbol{\beta}}^{(p)})$, one can evaluate the accuracy of indirect selection of the resulting SI and an *optimal rank* for the PC-SI can be chosen to maximize the accuracy of indirect selection.

Penalized selection indices. In a penalized regression, regularization is achieved by including in the objective function a penalty on model complexity. In the context of a SI, we have

$$\widehat{\boldsymbol{\beta}} = \arg\min_{\beta} \left\{ \frac{1}{2} \mathbb{E}\left(g_{y_i} - \boldsymbol{x}_i'\boldsymbol{\beta}\right)^2 + \lambda J(\boldsymbol{\beta}) \right\}, \tag{3}$$

where λ is a penalty parameter ($\lambda = 0$ yields the coefficients for the canonical SI) and $J(\boldsymbol{\beta})$ is a penalty function. Commonly used penalties include the L2 ($\|\boldsymbol{\beta}\|_2^2 = \sum_{j=1}^{p} \beta_j^2$) and L1 ($\|\boldsymbol{\beta}\|_1 = \sum_{j=1}^{p} |\beta_j|$) norms[17], or a weighted sum of the two[18].

Using $J(\boldsymbol{\beta}) = \frac{1}{2}\sum_{j=1}^{p} \beta_j^2$ in equation (3) renders a **Ridge-regression-type PSI** (RR-PSI, see *Methods*):

$$\widehat{\boldsymbol{\beta}}^{L2} = (\boldsymbol{P}_x + \lambda \boldsymbol{I})^{-1} \boldsymbol{G}_{x,y},$$

121 where $\boldsymbol{I}$ is a $p \times p$ identity matrix. The RR-PSI (referred to as the L2-PSI) yields shrunken estimates
122 of the regression coefficients.

123 In many applications, variable selection (i.e., a SI that is a function of a subset of the
124 measured phenotypes) may be desirable. This property can be obtained using penalties involving
125 the L1-norm, either alone, $J(\boldsymbol{\beta}) = \sum_{j=1}^{p} |\beta_j|$ (LASSO[19]), or in combination with the L2-norm,
126 $J(\boldsymbol{\beta}) = \frac{1}{2}(1-\alpha)\sum_{j=1}^{p}\beta_j^2 + \alpha\sum_{j=1}^{p}|\beta_j|$ (elastic-net[18]). Unlike the L2-PSI, the LASSO and elastic-
127 net SIs (hereinafter referred to as L1-PSI and EN-PSI, respectively) do not have a closed-form
128 solution[14]. However, solutions for PSIs involving an L1-penalty can be obtained using iterative
129 procedures such as the coordinate descent[20] and the least angle regression[21] (LARS) algorithms
130 (see *Methods*). As with the PC-SI, an optimal PSI can be obtained by choosing the values of the
131 regularizing parameters (λ, α) that maximize the accuracy of indirect selection.

132 **Accuracy of indirect selection**

133 Indirect selection accuracy is defined as the correlation between the index used to rank
134 genotypes and the genetic merit of the selection objective, that is, $Acc(I) = cor(I_i, g_{y_i})$. This
135 parameter is equal to the product of the square root of the heritability of the SI (h_I) times the
136 genetic correlation between the SI and the selection target, $cor(g_{I_i}, g_{y_i})$[16]. To avoid estimation
137 bias $Acc(I)$ must be estimated using data that was not used to derive the coefficients of the
138 index (Fig. 1); therefore, in the application presented below we: (*i*) partitioned the data into
139 training and testing sets, (*ii*) derived the coefficients of the SI in the training set, (*iii*) applied these
140 coefficients to image data of the testing set ($I_i = \boldsymbol{x}_i'\boldsymbol{\beta}$), and (*iv*) estimated h_I, $cor(g_{I_i}, g_{y_i})$, and

$Acc(I)$ in the testing set. Furthermore, we quantified the efficiency of indirect selection relative to mass phenotypic selection (RE) using $RE = \frac{h_I}{h_y} cor(g_{I_i}, g_{y_i})$[16].

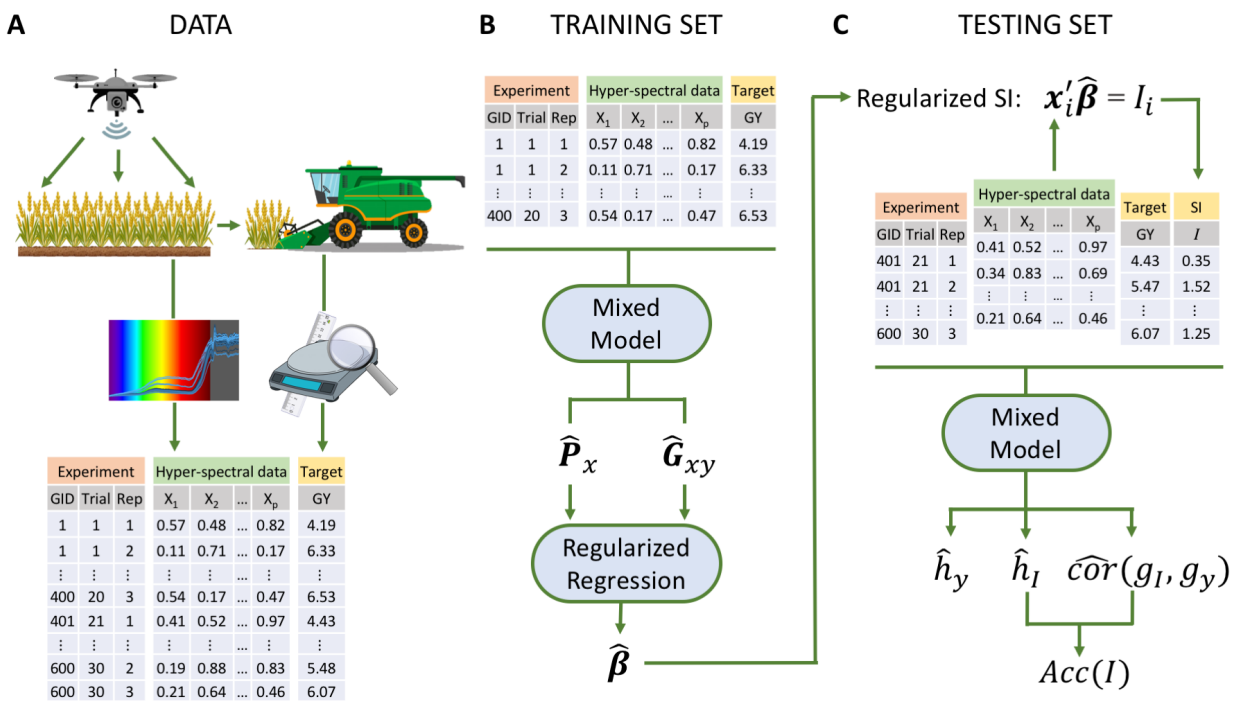

Figure 1. Prediction of the genetic merit for grain yield using hyper-spectral crop image data. (A) Data consists of hyper-spectral reflectance data ($\boldsymbol{x}_i$) and phenotypic measurements of the target trait (y_i, e.g., grain yield). (B) A subset of the data (the training set) is used to derive the coefficients ($\boldsymbol{\beta}$) of a selection index. (C) These coefficients are then applied to image data of individuals in the testing set to derive the index (I_i) for each individual. The predictive ability of the index is assessed by calculating the accuracy of indirect selection ($Acc(I)$) in the testing set.

153 **Regularized selection indices for wheat grain yield using hyper-spectral image data**

154 We applied the methodology described in the previous section to data (n=3,276) from the
155 CIMMYT's Global Wheat Program consisting of grain yield ($\mathrm{ton\ ha^{-1}}$) and hyper-spectral image
156 data. The data were collected at CIMMYT's experimental station in Ciudad Obregon, Sonora,
157 Mexico (27°20' N, 109°54' W, 38 masl) from 39 yield trials in which a total of 1,092 genotypes
158 were tested. Rainfall in Obregon is very limited; therefore, four different environments were
159 generated representing a combination of planting methods (*Flat* or *Bed*), controlled irrigation
160 (minimal, 2 or 5 irrigations), and planting dates (optimum or early-heat). As expected, average
161 yield decreased as drought stress intensity increased (see Table 1 and Supplementary Fig. S1 for
162 boxplots of yield by environment).

163

164 **Table 1 .** Average grain yield and heritability by environmental condition

Planting conditions		Number of irrigations	Abbreviation	Average (SD) Yield	Heritability (SD)
Date	System				
	Flat	Minimal	Flat-Drought	2.06 (0.58)	0.83 (0.016)
Optimum		2	Bed-2IR	3.67 (0.43)	0.66 (0.032)
	Bed	5	Bed-5IR	6.11 (0.61)	0.43 (0.025)
Early		5	Bed-EHeat	6.43 (0.73)	0.61 (0.018)

165 SD: standard deviation.

166

167 Image data was collected using an infrared and an hyper-spectral camera and consisted
168 of reflectance of electromagnetic power at 250 wavebands within the visible and near-infrared
169 spectrums (392-850 nm). Separate images were collected at 9 time-points covering vegetative
170 (VEG), grain filling (GF), and maturity (MAT) stages of the crop (see Supplementary Fig. S2). Grain
171 yield and image data were pre-adjusted using mixed-effects model that accounted for genotype,
172 trial, replicate, and sub-block (see *Methods* section).

173 **Regularization improves the heritability and the accuracy of the index**

174 To assess the effect of regularization on the accuracy of indirect selection we fitted an L1-PSI over
175 a grid of values of the regularization parameter ($\lambda^{(1)} > \lambda^{(2)} > \cdots > 0$ in equation (3), using $\lambda =$
176 0 renders a canonical SI). For each of the solutions ($\widehat{\boldsymbol{\beta}}(\lambda^{(1)})$, $\widehat{\boldsymbol{\beta}}(\lambda^{(2)})$,…) we estimated the
177 heritability of the resulting index and the genetic correlation between the index and the selection
178 target, and from those estimates we derived the accuracy of indirect selection. The same
179 approach was used to evaluate the accuracy of indirect selection of PC-SIs with a varying number
180 (1, 2, …) of PCs.

181 We first fitted PSIs and PC-SIs using data from a single time-point; the results from the
182 latest time-point (corresponding to MAT or late GF stages depending on the environment) are
183 presented in Fig. 2 (see Supplementary Figs. S3-S5 for other time-points). The heritability of the
184 L1-PSI (Fig. 2A) decreased as more bands became active in the index. Likewise, the heritability of
185 PC-SI (Fig. 2B) decreased with the number of PCs used. However, the genetic correlation
186 increased as either more bands become active in the L1-PSI or more PCs were used in the PC-SI.
187 Consequently, the maximum accuracy of indirect selection was achieved with a SI of intermediate

188 complexity (with anywhere between 20 and 60 of the 250 bands being active in the L1-PSI, and
189 between 20-60 PCs in the PC-SI). Results for other time-points and environments (Supplementary
190 Figs. S3-S5) exhibited similar patterns with some differences between environments. The
191 accuracy of indirect selection of the optimal L1-PSI was always close to that of the optimal PC-SI
192 and that of the optimal L2-PSI (Supplementary Table S1). Importantly, in all cases the accuracy of
193 indirect selection of the optimal regularized SIs was considerably higher than that of the
194 canonical SI, which is the one corresponding to 250 active bands or 250 PCs (i.e., the right-most
195 results in the plots in Fig. 2).

196

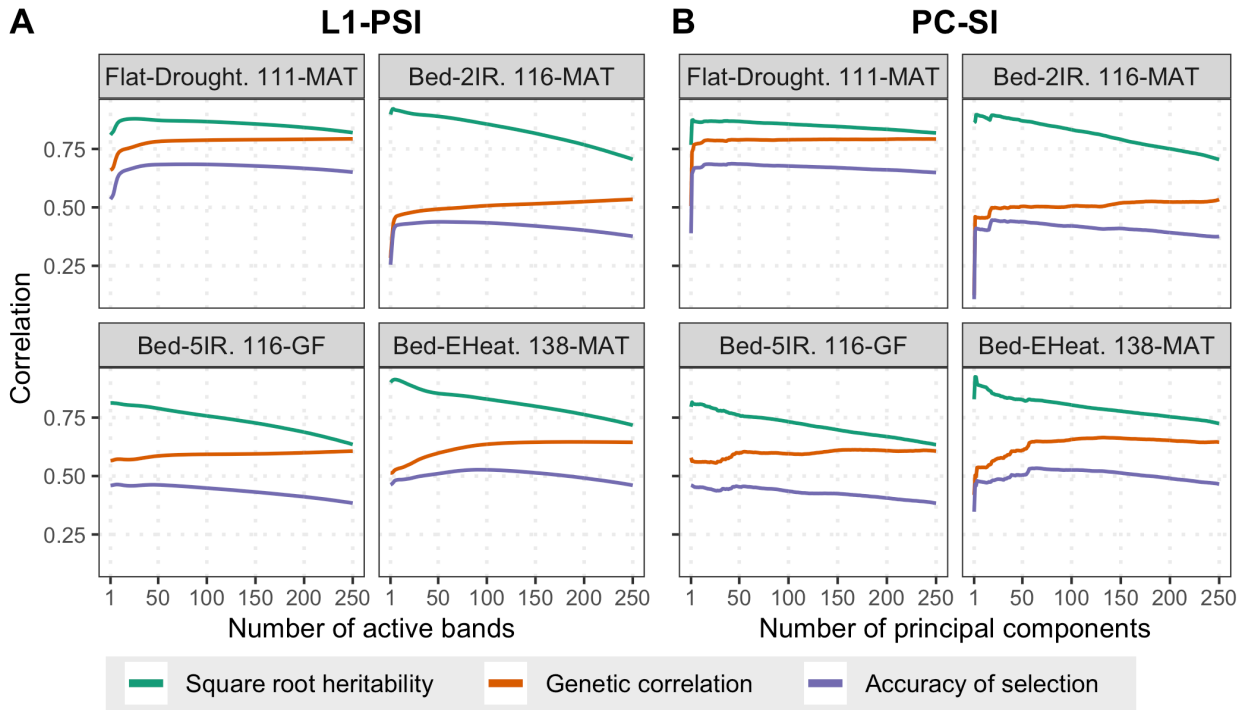

197

198 **Figure 2.** Accuracy of indirect selection of regularized SIs and its components. Square root
199 heritability (green), genetic correlation (orange), and accuracy of indirect selection (purple, all
200 averaged over 100 training-testing partitions), versus the number of predictors used to build the

201 index: (A) number of active bands in the case of the L1-PSI, or (B) number of PCs in the PC-SI.
202 Each panel represents one environment (latest time-point).

203

204 Fig. 3 displays the accuracy of indirect selection across time-points for the optimal (i.e.,
205 the one with the highest accuracy of indirect selection) L1-PSI and PC-SI. For comparison we also
206 display in the plot the accuracy of indirect selection achieved by a canonical SI (in green). The
207 estimated 95% confidence intervals of the accuracy of the regularized SIs (either PC-SI or L1-PSI)
208 are all above (and do not overlap) with the confidence intervals for the accuracy of the canonical
209 SI, except for a single time-point (57 DAS in environment *Bed-2IR*). Results from Tukey's Honest
210 Significance Difference confirmed that the accuracy of the regularized SIs is statistically different
211 (higher) than the canonical SI at a 5% of significance (Supplementary Table S1) for all but one (57
212 DAS in environment *Bed-2IR*) time-point/environment. Regularization increased the selection
213 accuracy across time-points and environments. Regularized SIs (either PC-SI or L1-PSI) had an
214 accuracy of indirect selection that was in average 10-40% higher than the accuracy achieved by
215 a canonical SI. These gains in accuracy were stronger in the optimal environment (*Bed-5IR* with a
216 median of 36%) and smaller in the stressed environments (*Flat-Drought* and *Bed-EHeat* with a
217 median of 16%). Interestingly, there were no sizable differences between the accuracy of indirect
218 selection achieved with the optimal L1-PSI and that of the optimal PC-SI. Compared with the
219 canonical SI, regularized SIs had higher heritability (Supplementary Fig. S6); this was achieved
220 without compromising the genetic correlation (Supplementary Fig. S7), thus leading to a higher
221 accuracy of indirect selection achieved by either penalization or rank-reduction strategies.

222

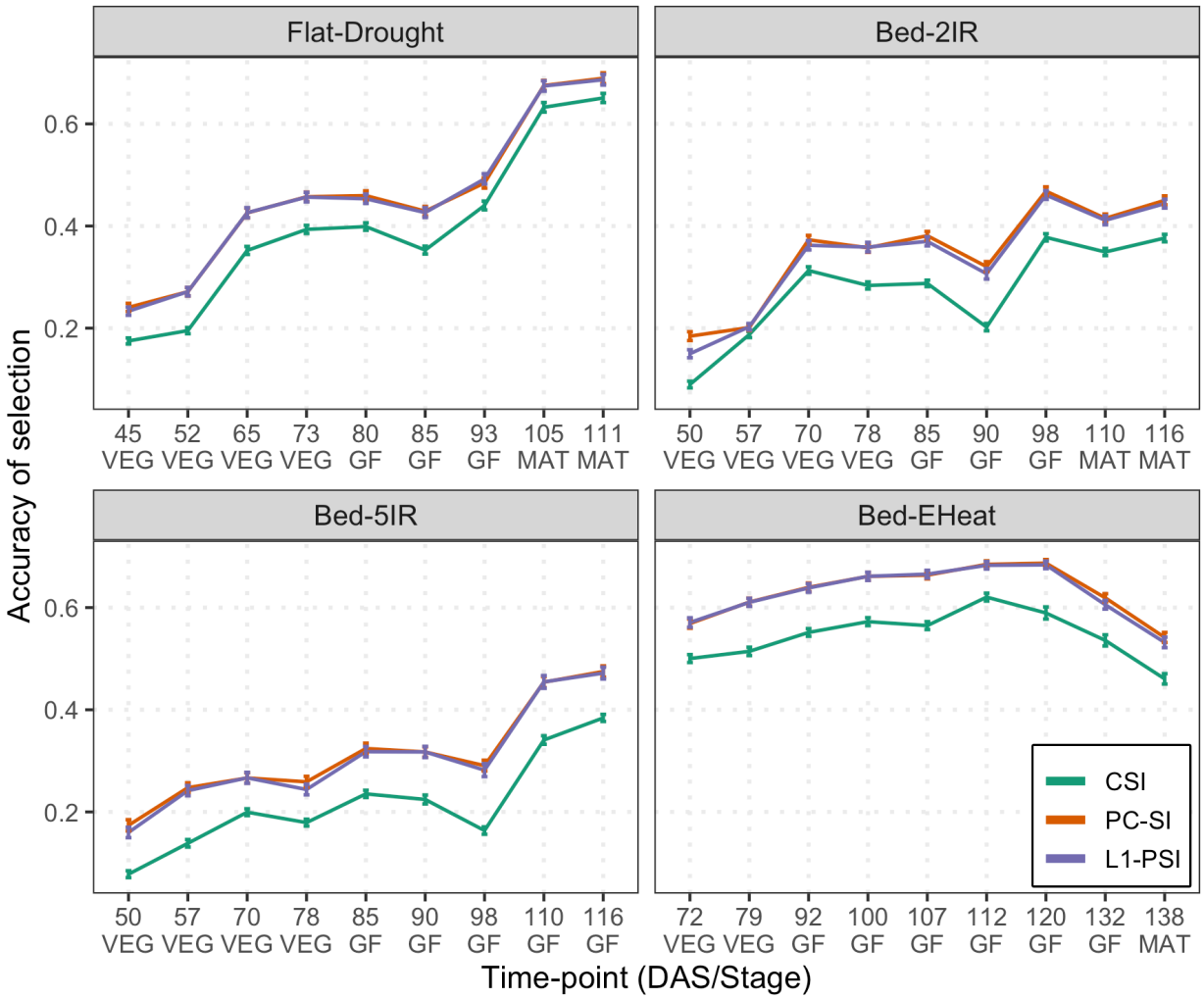

Figure 3. Accuracy of indirect selection achieved by a canonical (CSI) and by regularized (PC-SI and L1-PSI) selection indices. The lines provide the average accuracy over 100 training-testing partitions. Vertical lines represent a 95% confidence interval for the average. The horizontal axis give the time-point at which images were collected and are expressed in both days after sowing (DAS) and stages (VEG=vegetative, GF=grain filling, MAT=maturity).

232 **Using data from multiple time-points further improves selection accuracy**

233 The results presented above were based on data from a single time-point. We also generated
234 selection indices using data from multiple time-points (in this case, $\boldsymbol{x}_i$ was a vector containing
235 2,250 traits, corresponding to 250 wavebands measured at each of 9 time-points). Integrating
236 data from multiple time-points further increased the accuracy of L1-PSI by a margin that ranged
237 from 1 to 8 points on the correlation scale (Table 2). The gains in selection accuracy obtained
238 using data from multiple time-points were more evident in environments with lower accuracy;
239 similar results were obtained for the PC-SI and L2-PSI (Supplementary Table S1).

240

241 **Table 2.** Accuracy and relative efficiency of indirect selection of an L1-penalized SI using data
242 from one and nine time-points.

	Accuracy (SD)		Relative Efficiency (SD)	
Environment	Best single time-point*	Nine time-points combined	Best single time-point*	Nine time-points combined
Flat-Drought	0.69 (0.05)	0.70 (0.05)	0.74 (0.05)	0.75 (0.05)
Bed-2IR	0.46 (0.04)	0.54 (0.03)	0.57 (0.05)	0.67 (0.04)
Bed-5IR	0.47 (0.06)	0.55 (0.05)	0.72 (0.08)	0.83 (0.08)
Bed-EHeat	0.68 (0.04)	0.71 (0.04)	0.88 (0.05)	0.91 (0.04)

243 Values are presented as an average across 100 training-testing partitions. SD: standard deviation.
244 *For each environment we include the time-point that gave the highest accuracy of selection (see
245 Fig. 3 for other time-points).

246 **L1-penalization leads to sparse selection indices**

247 Fig. 4 shows a heatmap for the solutions of the optimal L1-PSI that integrated data from the 9
248 time-points. Each panel represents an environment, horizontal bands represent time-points.
249 Within each time-point wavebands not entering in the solution are in grey and non-zero
250 coefficients are represented in a yellow-red scale (red indicates large absolute-value
251 coefficients). The well-irrigated environments (*Bed-5IR* and *Bed-EHeat*) had considerably sparser
252 indices with only a reduced number of wavebands in the solutions; these were mostly located in
253 the violet, blue and red regions of the spectrum. In stressed environments (*Flat-Drought* and *Bed-*
254 *2IR*) there were also a few wavebands in the green and infrared regions that were active. In all
255 the indices, there were wavebands from several time-points that were active in the optimal
256 solution, suggesting that data from both early and late phenological stages are informative about
257 the genetic merit for grain yield.

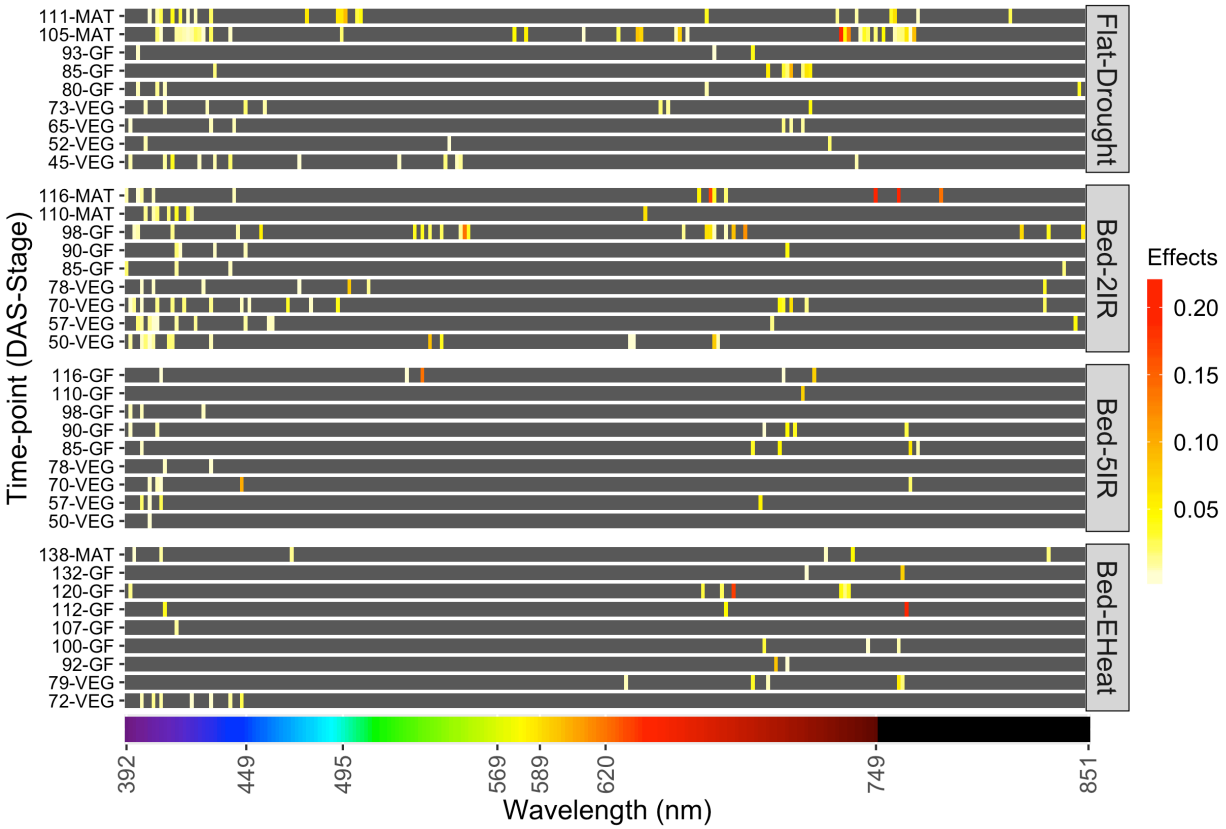

Figure 4. Heatmap of regression coefficients for L1-penalized selection indices. Separate indices were derived for each environment using multi time-point data. DAS=days after sowing, VEG, GF, MAT represent vegetative, grain-filling and maturity stages, respectively. The bottom color-bar shows the light color associated with each waveband in the visible spectrum (≤ 750 nm); black was used to represent the near-infrared spectrum (wavelength > 750 nm).

Comparison with phenotypic prediction

We compared the accuracy of indirect selection of the PSI and PC-SI with vegetation indices and penalized phenotypic prediction. Vegetation indices are often used to predict yield[22], biomass, and chlorophyll content[23,24]. We considered two vegetation indices: the Red and Green

269 Normalized Difference Vegetation Indices (RNDVI[25] and GNDVI[26] respectively). For each of these
270 indices we estimated the genetic correlation with grain yield, as well as their heritability and
271 accuracy of indirect selection (Supplementary Table S1). Overall, the accuracy of indirect
272 selection of the GNDVI and RNDVI was lower than the one achieved with a PSI (the average
273 difference in accuracy between RNDVI and the L1-PSI varied by environment from 0.02 to 0.14
274 points in correlation, Supplementary Table S1, in favor of the L1-PSI). The heritability of the
275 GNDVI and RNDVI was similar and superior in some cases to that of the L1-PSI (Supplementary
276 Fig. S6); however, the genetic correlation between the vegetation indices and grain yield was (in
277 most time-points and environments) lower than the genetic correlation between the L1-PSI and
278 grain yield (Supplementary Fig. S7). Thus, the main driver of the difference in accuracy between
279 the L1-PSI and the vegetation indices was the difference in genetic correlation.

280 We also fitted L1-penalized phenotypic prediction (L1-Phen) and compared the accuracy
281 of indirect selection of these phenotypic prediction methods with that of penalized SIs. Overall,
282 the L1-Phen achieved an accuracy of indirect selection very close to that of the L1-PSI
283 (Supplementary Table S1); however, in a few environments at some time-points, the L1-PSI
284 achieved a higher accuracy of indirect selection than the phenotypic prediction.

285

286 **Discussion**

287 High-throughput phenotyping has been extensively adopted in agricultural research and
288 commercial production. Extracting interpretable information from HTP data poses important
289 statistical challenges. The clear majority of research in this area has focused on calibrating

290 equations to predict phenotypes (e.g., total biomass, grain yield) using HTP data as inputs. This
291 approach is well-suited for phenotypic prediction; however, the same approach can be sub-
292 optimal for selection because the best predictor of a phenotype is not always the best predictor
293 of the genetic merit of the same trait.

294 The best (linear) phenotypic predictor is the sum of the best linear predictor of the genetic
295 merit (g_y) plus the best linear predictor of the environmental term (ε_y), that is, $\mathbb{E}(y|\boldsymbol{x}) =$
296 $\mathbb{E}(g_y|\boldsymbol{x}) + \mathbb{E}(\varepsilon_y|\boldsymbol{x})$. The first term, $\mathbb{E}(g_y|\boldsymbol{x})$, is the SI and it is, by construction, maximally
297 correlated with the genetic merit. The second term, $\mathbb{E}(\varepsilon_y|\boldsymbol{x})$, is relevant for phenotypic
298 prediction but represents noise when the problem is that of selecting the best genotypes.

299 Selection indices exploit genetic covariances, while phenotypic prediction relies on
300 phenotypic covariances between the selection target and the measured phenotype (e.g., crop
301 imaging). Thus, the two methods yield different results whenever the patterns of phenotypic
302 correlations are sufficiently different from the patterns of genetic correlations. In our data set,
303 environmental conditions were highly controlled, with relatively low un-controlled within-trial
304 variability in environmental conditions. Consequently, the patterns of phenotypic and genetic
305 correlations were very similar (see Supplementary Fig. S8). This was true for many time-points
306 and environments but not in others (e.g., 80, 85 and 93 DAS in *Flat-Drought*, and 90 and 98 DAS
307 in *Bed-2IR*); it was exactly in those time-points and environments that the L1-PSI achieved higher
308 accuracy of indirect selection than the L1-Phen method (Supplementary Table S1).

309 A canonical SI (equation (1)) is, by construction, maximally correlated with the genetic
310 merit of the selection objective. This optimality property holds when the genetic and phenotypic

311 (co)variance matrices that are needed to derive the coefficients of the SI (see equation (2)) are
312 known without error. However, when the measured phenotype is high-dimensional, estimation
313 errors in the phenotypic (co)variance matrix ($\boldsymbol{P}_x$), as well as in the genetic covariances ($\boldsymbol{G}_{x,y}$), can
314 make the canonical SI sub-optimal. Our empirical results confirm this: canonical SIs over-fitted
315 the data; this leads to a SI with low heritability and low accuracy of indirect selection.

316 To prevent overfitting, we considered integrating ideas commonly used in high-
317 dimensional regression into the SI methodology. Our empirical results show that regularization
318 consistently improves the accuracy of indirect selection relative to canonical SIs. We verified this
319 for various environmental conditions and for crop imaging data collected at 9 different time-
320 points. The optimal PSI and the optimal PC-SI achieved almost the same accuracy of indirect
321 selection for all the environments and time-points, suggesting that either type of regularization
322 can be effective.

323 Reduced-rank selection indices are appealing because after dimension reduction the
324 problem of deriving a SI is trivial and can be dealt with methods commonly used to derive
325 canonical SIs. Moreover, after HTP has been reduced to a few derived-traits (say the top 10 PCs),
326 these traits can be integrated into genetic evaluations (either pedigree-based[27] or genomic-
327 enabled[28]) using standard multi-trait models.

328 Principal components-based methods have been considered before in the analysis of
329 Fourier-transformed infrared (FTIR) spectra derived from milk samples. For instance, Soyeurt,
330 Misztal & Gengler[29] used a reduced number of FTIR-derived PCs to estimate variance components
331 for selection objectives (e.g., fat or protein content in milk). Building upon this idea, Dagnachew,

332 Meuwissen & Ådnøy[30] suggested predicting the genetic merit for milk fatty acids using FTIR-
333 derived PCs as 'traits' in a genetic evaluation. However, when mapping from genetic predictions
334 of PC-lodgings onto genetic predictions for the selection objective the authors used coefficients
335 derived from a phenotypic (partial least squares) regression. This does not guarantee that the
336 resulting index is maximally correlated with the genetic merit of the selection target. The
337 penalized and PC-SI presented in this study address that problem by using coefficients that are
338 derived using genetic (and not phenotypic) covariances.

339 A disadvantage of the PC-SI is that the methodology does not naturally provide variable
340 selection, a feature that may be desirable when the measured phenotype is high-dimensional.

341 Penalized selection indices can perform variable selection based on genetic covariances.
342 While the derivation of a PSI is a bit more challenging than that of the PC-SI, the computational
343 burden involved in the derivation of a PSI is not extremely high.

344 **Integration of PSI and PC-SI into genetic evaluations.** The SIs considered here predict genetic
345 merit for a selection target from a set of traits measured on an individual ($I_i = \boldsymbol{x}_i'\boldsymbol{\beta}$); such indices
346 exploit borrowing of information between traits within an individual. Borrowing of information
347 between individuals increases selection accuracy; we envision two ways in which regularized SIs
348 can be integrated into pedigree or genomic-based genetic evaluations.

349 One possibility is to use **a two-steps approach** whereas in the first step a PSI or a PC-SI is
350 used to predict the genetic merit using within-individual information. This step can be considered
351 as a task where patterns attributable to genetic covariances are extracted and those attributable

352 to environmental covariances are smoothed-out. Then, in a second step, the resulting index-data
353 $\{I_1, \dots, I_n\}$ could be used as a trait in a genetic evaluation.

354 A **one-step** approach is also conceptually possible: the optimization problem of equation
355 (3) can be modified by replacing $\boldsymbol{x}_i$, the vector with the measured phenotypes on the ith
356 individual, with a vector $\boldsymbol{x} = (\boldsymbol{x}_1', \boldsymbol{x}_2', \dots, \boldsymbol{x}_n')'$ that contains all the available HTP data (measured
357 on all n individuals); after expanding the squared error loss and taking expectations we get

358 $$\widehat{\boldsymbol{\beta}}_i = \arg\min_{\boldsymbol{\beta}_i} \left\{ \frac{1}{2}\mathbb{E}\left(g_{y_i}^2\right) - \boldsymbol{\beta}_i'\boldsymbol{G}_{gx} + \frac{1}{2}\boldsymbol{\beta}_i'\boldsymbol{P}_x\boldsymbol{\beta}_i + \lambda J(\boldsymbol{\beta}_i) \right\},$$

359 where $\boldsymbol{G}_{gx}$ is a $pn \times 1$ vector of genetic covariances including between-traits-within-individual
360 (co)variances and between-subjects covariances. In standard genetic models, $\boldsymbol{G}_{gx}$ takes a
361 Kronecker form $\boldsymbol{G}_{gx} = \boldsymbol{A}_i \circ \boldsymbol{G}_{x,y}$, where $\boldsymbol{A}_i$ are genetic (either DNA- or pedigree-derived)
362 relationships between the candidate for selection and each of the individuals in the training set,
363 and $\boldsymbol{G}_{x,y}$ is, as before, a vector of genetic covariances between the selection objective and the
364 measured traits ($\boldsymbol{x}$). Likewise, $\boldsymbol{P}_x$ is a $pn \times pn$ phenotypic (co)variance matrix. Estimating $\boldsymbol{P}_x$
365 would require estimating all the genetic and environmental covariances among the measured
366 traits. Therefore, while a one-step approach is conceptually feasible, the implementation can be
367 computationally challenging.

368 **Impact of the use of high-throughput phenotypes in breeding programs**. According to breeders'
369 equation[16,31], the rate of genetic gain from selection is directly proportional to selection accuracy
370 and selection intensity. Thus, relative to the use of canonical SIs, the use of regularized SIs is
371 expected to increase selection gains by a factor equal to the gains observed in accuracy, that is
372 between 10% and 40%. Relative to mass phenotypic selection, the PSIs had efficiencies, RE,

373 ranging from 60% to 90%; therefore, relative to direct phenotypic selection, selection decisions
374 based on PSI derived from images are expected to yield lower genetic gains than the ones that
375 could be achieved via direct mass selection. However, the use of HTP technologies (e.g., crop
376 monitoring using hyper-spectral cameras mounted in drones) may enable the expansion of the
377 number of genotypes tested/measured as well as the number of locations where those
378 genotypes are tested. This could lead to an increase in selection intensity which will in turn
379 increase selection gains. For instance, if the use of HTP enables doubling the number of
380 genotypes tested, the increase in selection gains that could be achieved with HTP may range from
381 20% (in the case where the PSI has RE of 60%) to 80% (for the traits/environments with RE of
382 90%).

383 **Regularized selection indices can also be a valuable tool in genetic research**. High-dimensional
384 phenotypes are also becoming increasingly available in genetic studies involving human subjects
385 and model organisms. Performing genetic studies (e.g., genome-wide association analyses) on
386 high-dimensional phenotypes is challenging and the burden of multiple testing across hundreds
387 or thousands of phenotypes (e.g., RNA-abundance across thousands of genes) may critically
388 compromise power. The PSI and PC-SI presented in this study could be used to extract genetic
389 patterns from high dimensional phenotype data such as brain imaging or whole-genome gene
390 expression profiles and these patterns can then be used as traits in genetic studies.

391 **Conclusion**. We proposed two novel methods for predicting the genetic merit for selection
392 objectives from high-dimensional phenotypes. These phenotypes are becoming increasingly
393 available as the adoption of HTP in crop and animal production increases. The proposed methods
394 integrate regularization procedures commonly used in high-dimensional regressions into the SI

methodology. Regularization prevents overfitting and increases the accuracy of the index. The methods proposed here can be used to extract genetic patterns from almost any kind of high-dimensional phenotype, including not only HTP data emerging in agriculture but also high-dimensional phenotypes that emerge in genetic studies involving human subjects and model organisms.

Methods

Canonical selection index

The weights on a SI are derived as the solution to the optimization problem of equation (1):

$$\widehat{\boldsymbol{\beta}} = \arg\min_{\beta} \tfrac{1}{2}\,\mathbb{E}\left(g_{y_i} - \boldsymbol{x}_i'\boldsymbol{\beta}\right)^2.$$

The right-hand side can be expressed as $\mathbb{E}\left(g_{y_i} - \boldsymbol{x}_i'\boldsymbol{\beta}\right)^2 = \mathbb{E}\left(g_{y_i}^2\right) - 2\,\mathbb{E}\left(g_{y_i}\boldsymbol{x}_i\right)'\boldsymbol{\beta} + \boldsymbol{\beta}'\mathbb{E}(\boldsymbol{x}_i\boldsymbol{x}_i')\boldsymbol{\beta}$. The first term, $\mathbb{E}\left(g_{y_i}^2\right)$, does not involve $\boldsymbol{\beta}$; therefore, it can be dropped from the objective function. Furthermore, if $\boldsymbol{x}_i$ has null mean, and assuming that the environmental effects on $\boldsymbol{x}_i$ are orthogonal to g_{y_i}, then $\mathbb{E}\left(g_{y_i}\boldsymbol{x}_i\right) = \boldsymbol{G}_{x,y}$ is a vector containing the genetic covariances between the selection target and each of the measured phenotypes. Likewise, $\mathbb{E}(\boldsymbol{x}_i\boldsymbol{x}_i') = \boldsymbol{P}_x$ is the phenotypic (co)variance matrix of $\boldsymbol{x}_i$. Therefore, the problem in equation (1) can be written as

$$\widehat{\boldsymbol{\beta}} = \arg\min_{\beta} \left\{-\boldsymbol{G}_{x,y}'\boldsymbol{\beta} + \tfrac{1}{2}\boldsymbol{\beta}'\boldsymbol{P}_x\,\boldsymbol{\beta}\right\}.$$

Differentiating the right-hand side with respect to vector $\boldsymbol{\beta}$ and setting the derivatives equal to zero leads to the first order conditions: $\boldsymbol{P}_x\widehat{\boldsymbol{\beta}} = \boldsymbol{G}_{x,y}$; therefore,

$$\widehat{\boldsymbol{\beta}} = \boldsymbol{P}_x^{-1}\boldsymbol{G}_{x,y}.$$

Reduced-rank selection index

Recall that the singular value decomposition of a real-valued matrix, $\boldsymbol{X} = [\boldsymbol{x}_1, \boldsymbol{x}_2, \dots, \boldsymbol{x}_n]'$ (individuals in rows, phenotypes in columns) takes the form $\boldsymbol{X} = \boldsymbol{UDV}'$, where $\boldsymbol{U} = [\boldsymbol{u}_1, \dots, \boldsymbol{u}_p]$ is the matrix containing the left-singular vectors that span the row-space of $\boldsymbol{X}$, $\boldsymbol{V} = [\boldsymbol{v}_1, \dots, \boldsymbol{v}_p]$ is the matrix with the right-singular vectors, and $\boldsymbol{D} = \mathrm{diag}(d_1, \dots, d_p)$ is a diagonal matrix with positive or zero elements. The PCs $\boldsymbol{W} = \boldsymbol{XV} = \boldsymbol{UD}$ are linear combinations of the measured phenotypes. A reduced-rank regression uses the first q PCs ($\widetilde{\boldsymbol{W}} = [\boldsymbol{w}_1, \dots, \boldsymbol{w}_q]$, $q \leq p$) as 'measured phenotypes' in the SI:

$$\widehat{\boldsymbol{\gamma}}^{(q)} = \arg\min_{\gamma} \tfrac{1}{2}\mathbb{E}\left(g_{y_i} - \widetilde{\boldsymbol{w}}_i'\boldsymbol{\gamma}^{(q)}\right)^2,$$

where $\widetilde{\boldsymbol{w}}_i$ is a vector containing the scores for the ith observation on the first q PCs. The solution to the optimization problem takes the form $\widehat{\boldsymbol{\gamma}}^{(q)} = \boldsymbol{P}_{\widetilde{w}}^{-1}\boldsymbol{G}_{\widetilde{w},y}$, where $\boldsymbol{P}_{\widetilde{w}}$ is the phenotypic (co)variance matrix of the first q PCs and $\boldsymbol{G}_{\widetilde{w},y}$ is a vector containing the genetic covariances between each of the top q PCs and the selection objective. Since the left-singular vectors are orthonormal (i.e., $\boldsymbol{u}_j'\boldsymbol{u}_j = 1$ and $\boldsymbol{u}_j'\boldsymbol{u}_k = 0$, for $j \neq k$), then $\boldsymbol{W}'\boldsymbol{W} = \boldsymbol{D}^2 = \mathrm{diag}(d_1^2, \dots, d_p^2)$. Hence, a method-of-moments estimate of the phenotypic (co)variance matrix of $\widetilde{\boldsymbol{W}}$ contains only the first q elements $\widetilde{\boldsymbol{D}}^2 = \mathrm{diag}(d_1^2, \dots, d_q^2)$; this is

$$\widehat{\boldsymbol{P}}_{\widetilde{w}} = \frac{1}{n-1}\widetilde{\boldsymbol{D}}^2.$$

Using $\widehat{\boldsymbol{P}}_{\widetilde{w}}$ makes the coefficients of the PCs to be proportional to the genetic covariance between each of the PCs and the selection objective: $\widehat{\boldsymbol{\gamma}}^{(q)} = (n-1)(\widetilde{\boldsymbol{D}}^2)^{-1}\boldsymbol{G}_{\widetilde{w},y}$. This solution can be mapped to coefficients for the measured traits using $\widehat{\boldsymbol{\beta}}^{(q)} = (n-1)\widetilde{\boldsymbol{V}}(\widetilde{\boldsymbol{D}}^2)^{-1}\boldsymbol{G}_{\widetilde{w},y}$, where $\widetilde{\boldsymbol{V}}$ is the matrix containing only the first q right-singular vectors.

Penalized selection indices

The objective function of the penalized SI is given by equation (3). Here we considered PSIs using either L1 or L2-norms or a combination of the two.

L2-PSI. Using an L2-norm as penalty, $J(\boldsymbol{\beta}) = \frac{1}{2}\sum_{j=1}^{p}\beta_j^2 = \frac{1}{2}\boldsymbol{\beta}'\boldsymbol{\beta}$, in equation (3) leads to the following optimization problem:

$$\widehat{\boldsymbol{\beta}}^{L2} = \arg\min_{\beta}\left\{\frac{1}{2}\mathbb{E}\left(g_{y_i} - \boldsymbol{x}_i'\boldsymbol{\beta}\right)^2 + \lambda\frac{1}{2}\boldsymbol{\beta}'\boldsymbol{\beta}\right\}.$$

Therefore:

$$\widehat{\boldsymbol{\beta}}^{L2} = \arg\min_{\beta}\left\{-\boldsymbol{G}_{x,y}'\boldsymbol{\beta} + \frac{1}{2}\boldsymbol{\beta}'\boldsymbol{P}_x\,\boldsymbol{\beta} + \lambda\frac{1}{2}\boldsymbol{\beta}'\boldsymbol{\beta}\right\}.$$

The second and third right-hand side terms can be combined to obtain:

$$\widehat{\boldsymbol{\beta}}^{L2} = \arg\min_{\beta}\left\{-\boldsymbol{G}_{x,y}'\boldsymbol{\beta} + \frac{1}{2}\boldsymbol{\beta}'(\boldsymbol{P}_x + \lambda\boldsymbol{I})\boldsymbol{\beta}\right\},$$

where $\boldsymbol{I}$ is a $p \times p$ identity matrix. Differentiating with respect to $\boldsymbol{\beta}$ and setting the derivatives equal to zero, we obtain the first-order conditions: $(\boldsymbol{P}_x + \lambda\boldsymbol{I})\widehat{\boldsymbol{\beta}}^{L2} = \boldsymbol{G}_{x,y}$; therefore:

449 $$\widehat{\boldsymbol{\beta}}^{L2} = (\boldsymbol{P}_x + \lambda \boldsymbol{I})^{-1}\boldsymbol{G}_{x,y}.$$

450 **EN-PSI**. The coefficients for the elastic-net family are obtained by considering an objective

451 function as in equation (3), with $J(\boldsymbol{\beta}) = \frac{1}{2}(1-\alpha)\sum_{j=1}^{p}\beta_j^2 + \alpha\sum_{j=1}^{p}|\beta_j|$; therefore,

452 $$\widehat{\boldsymbol{\beta}}^{EN} = \arg\min_{\beta}\left\{-\boldsymbol{G}'_{x,y}\boldsymbol{\beta} + \frac{1}{2}\boldsymbol{\beta}'\boldsymbol{P}_x\boldsymbol{\beta} + \lambda\frac{1}{2}(1-\alpha)\sum_{j=1}^{p}\beta_j^2 + \lambda\alpha\sum_{j=1}^{p}|\beta_j|\right\}.$$

453 The L1-PSI and L2-PSI are particular cases corresponding to $\alpha = 1$ and $\alpha = 0$, respectively. When

454 $\alpha = 0$ the solution has a closed-form (see L2-PSI above). If $\alpha > 0$, no closed-form solution exists;

455 however, a solution can be obtained using the same iterative algorithms that are used to solve

456 elastic-net regressions (e.g., LARS and coordinate descent[14]). These algorithms can be

457 implemented either by 'partial residuals' or using 'covariance updates'[32]. In our case, the

458 objective function is entirely based on (co)variance terms. The objects $\boldsymbol{P}_x$ and $\boldsymbol{G}_{x,y}$ enter in the

459 objective function of the PSI in the same way that $\boldsymbol{X}'\boldsymbol{X}$ and $\boldsymbol{X}'\boldsymbol{y}$ enter in a standard elastic-net

460 regression. Therefore, to obtain solutions, we implemented the standard LARS algorithm (e.g.,

461 Hastie *et al*.[14]) entirely based on covariance updates.

462 **Data**

463 The data set consists of 1,092 inbred wheat lines grouped into 39 trials and grown during the

464 2013-2014 season at the Norman Borlaug experimental research station in Ciudad Obregon,

465 Sonora, Mexico. Each trial consisted of 28 breeding lines that were arranged in an alpha-lattice

466 design with three replicates and six sub-blocks. The trials were grown in four different

467 environments: *Flat-Drought* (sowing in flat with irrigation of 180 mm through drip system), *Bed-*

468 *2IR* (sowing in bed with 2 irrigations approximately 250 mm), *Bed-EHeat* (bed sowing 30 days

469 before optimal planting date with 5 normal irrigations approximately 500 mm), and *Bed-5IR* (bed
470 sowing with 5 normal irrigations). In 2013, all the trials were planted by mid-November (optimal
471 planting date), on the 21st (*Bed-2IR* and *Bed-5IR*) and on the 26th for *Flat-Drought*. Trials for *Bed-*
472 *EHeat* were planted on October 30th. Grain yield ($\mathrm{ton\ ha^{-1}}$, total plot yield after maturity) was
473 recorded.

474 Reflectance data were collected from the fields using both infrared (A600 series Infrared
475 camera, FLIR, Wilsonville, OR) and hyper-spectral (A-series, Micro-Hyperspec, VNIR Headwall
476 Photonics, Fitchburg, MA) cameras mounted on a Piper PA-16 Clipper aircraft on 9 different dates
477 (time-points) between January 10th and March 27th, 2014. During each flight, data from $p =$
478 250 wavebands ranging from 392 to 850 nm were collected for each pixel in the pictures. Using
479 ArcMap software (ESRI, CA), the average reflectance of all the pixels within each geo-referenced
480 trial plot was calculated and reported as a single data-point for each genotype for each band.
481 Days to heading were recorded as the number of days from the date of sowing/first irrigation
482 until 50% of spike emergence in each plot. Heading of about 50-80% of the total number of plots
483 was used as criterion to distinguish between vegetative (VEG) and grain filling (GF) stages. The
484 crop was considered to be at maturity (MAT) stage when the average RNDVI decreased to ~0.4.

485 **Phenotype pre-processing**

486 Within each environment, grain yield phenotypic records were pre-adjusted by fitting the
487 following mixed model,

488 $$y_{jklm} = \mu + g_j + t_k + r_{l(k)} + b_{m(kl)} + \varepsilon_{jklm},$$

489 where y_{jklm} is the grain yield phenotype value for the jth genotype, k^{th} trial, l^{th} replicate (within

trial), m^{th} sub-block (within trial and replicate), μ is the overall mean and g_j, t_k, $r_{l(k)}$, and $b_{m(kl)}$ are the genotype, trial, replicate, and sub-block effects, respectively (all assumed to be random) and ε_{jklm} is an error term. Random effects were assumed to be independently and identically distributed (*iid*) normal with null mean and effect-specific variances. Likewise, the error terms were assumed to be *iid* with null mean and common error variance.

Grain yield data were pre-adjusted by subtracting from the phenotypic record (y_{jklm}) the mean ($\hat{\mu}$) plus BLUPs of trial, replicate, and sub-block effects; this is

$$y^*_{jklm} = y_{jklm} - \hat{\mu} - \hat{t}_k - \hat{r}_{l(k)} - \hat{b}_{m(kl)} = \hat{g}_j + \hat{\varepsilon}_{jklm}. \quad (4)$$

Reflectance data was pre-adjusted by fitting the above model, using reflectance at individual bands as phenotype expanded with the inclusion of a time-point effect. Separate models were fitted to each of the wavebands. As with grain yield, reflectance data were pre-adjusted by subtracting from the measured reflectance the estimated mean and predicted time-point, trial, replicate, and sub-block effects.

For quality control, pre-adjusted grain yield and reflectance phenotypes were removed for those grain yield scores lying beyond 3 times the inter-quantile region from the 0.25 and 0.75 quantiles.

After pre-adjusting, all phenotypes were standardized (to have unit variance); for ease of exposition, hereinafter we refer to the adjusted-scaled phenotypes (including grain yield and the image data) simply as phenotypes.

Heritability estimation

After pre-adjusting standardization, we analyzed phenotypes using a mixed model of the form

511 $$y_{ij} = g_j + \varepsilon_{ij}, \quad (5)$$

512 where y_{ij} is the phenotype for the ith observation (i here is a single index for indices k, l, and m

513 in equation (4)) of the jth genotype; the genetic values are $g_j \overset{iid}{\sim} N(0, \sigma^2_{g_y})$, where $\sigma^2_{g_y}$ is the

514 genetic variance; and the environmental terms are $\varepsilon_{ij} \overset{iid}{\sim} N(0, \sigma^2_{\varepsilon_y})$. Plot-basis heritability was

515 calculated from variance components estimates using

516 $$h^2_y = \frac{\sigma^2_{g_y}}{\sigma^2_{g_y} + \sigma^2_{\varepsilon_y}}.$$

517 **Training-testing partitions**

518 The data set contains information from 39 trials with 84 observations each. To assess the

519 accuracy of indirect selection, we randomly assigned complete trials to testing sets. The training

520 set comprised all the data from the trials not assigned to the testing set. This approach

521 guarantees that no data from a single trial is present in both training and testing sets. This

522 approach aims at representing a situation where one has calibrated the coefficients of the index

523 using historical trials and apply these coefficients to image data of future trials. A similar

524 validation scheme has been used (using herd-year-season groups instead of trials) in validation

525 problems in previous studies involving milk spectra data[33]. In each training-testing partition, out

526 of the 29 trials available, 26 trials ($n_{trn} \approx 2{,}184$ observations) were randomly assigned to the

527 training set, and the data from the remaining 13 trials ($n_{tst} \approx 1{,}092$) was used for testing set.

528 The regression coefficients of the indices (the $\boldsymbol{\beta}$'s for the canonical SI, PSI, and PC-SI) were

529 calculated using grain yield and reflectance data of the training set. Estimates of the coefficients

530 and reflectance data were then used to calculate the SI, $I_{ij} = \boldsymbol{x}'_{ij}\widehat{\boldsymbol{\beta}}$, for each observation i in the

testing set ($i = 1, \dots, n_{tst}$). The heritability of the index and the genetic correlation between the index and the selection goal were estimated in the testing set.

The training-testing procedure described above was repeated 100 times by randomly assigning trials to training and testing sets. From these analyses, we reported the mean of heritability, genetic correlation, and selection accuracy; and their standard deviation across training-testing partitions.

Estimation of phenotypic and genetic parameters

The population phenotypic (co)variance matrix $\boldsymbol{P}_x$ was estimated within the training set using the unbiased sample (co)variance matrix given by $\widehat{\boldsymbol{P}}_x = \frac{1}{n-1}\sum_{i=1}^{n_{trn}}(\boldsymbol{x}_i - \overline{\boldsymbol{x}})(\boldsymbol{x}_i - \overline{\boldsymbol{x}})'$, where $\overline{\boldsymbol{x}}$ is the vector containing the sample mean of each waveband. Since reflectance data are centered and standardized, this reduces to $\widehat{\boldsymbol{P}}_x = \frac{1}{n-1}\boldsymbol{X}'\boldsymbol{X}$, where $\boldsymbol{X} = [\boldsymbol{x}_1, \boldsymbol{x}_2, \dots, \boldsymbol{x}_n]'$ is the matrix containing all measured traits in the training set.

The genetic covariance ($G_{x_j,y}$) between grain yield and the jth measured trait ($j = 1, \dots, p$) was estimated using a sequence of univariate genetic models as in equation (5). We fitted that model with grain yield phenotypes as response, then for each of the reflectance bands and then for the sum of grain yield and each of the bands. The genetic covariances between the bands and grain yield were then estimated using

$$\widehat{\boldsymbol{G}}_{y,x_j} = \frac{1}{2}\left(\hat{\sigma}^2_{g_{y+x_j}} - \hat{\sigma}^2_{g_y} - \hat{\sigma}^2_{g_{x_j}}\right)',$$

where $\hat{\sigma}^2_{g_y}$, $\hat{\sigma}^2_{g_{x_j}}$ and $\hat{\sigma}^2_{g_{y+x_j}}$ are the estimated genetic variances for grain yield, the jth band, and the sum of grain yield and the jth band, respectively.

551 **Estimation of the accuracy of indirect selection**

552 To assess the accuracy of indirect selection we applied the regression coefficients derived in the
553 training set to image data from the testing set to derive $I_{ij} = \boldsymbol{x}'_{ij}\widehat{\boldsymbol{\beta}}$. Then, using a mixed model
554 analysis like that described in the previous section we estimated the heritability of the SI (h_I^2),
555 the heritability of grain yield (h_y^2), and the genetic correlation between the SI and grain yield
556 ($cor(g_{I_i}, g_{y_i})$). From these estimates, we derived the accuracy of indirect selection, $Acc(I) =$
557 $h_I\ cor(g_{I_i}, g_{y_i})$, and the relative efficiency, $RE = \frac{h_I}{h_y} cor(g_{I_i}, g_{y_i})$.

558 **Software**

559 All the aforementioned analyses were implemented in the R software environment[34], version
560 3.5.1. Linear mixed models were implemented using the 'lmer' function from the LME4[35] R-
561 package. Code that implements LARS in the context of SIs was programed based on the LARS[36] R-
562 package.

563 **Materials and data availability**

564 The data used in this study are publicly available by CIMMYT (https://www.cimmyt.org/) who
565 owns all rights in the data. Data sets and R-scripts that perform all analyses are publicly available
566 upon request to the corresponding author.

567

568

569

570 # References

571 1. Nagel, K. A. *et al.* GROWSCREEN-Rhizo is a novel phenotyping robot enabling simultaneous
572 measurements of root and shoot growth for plants grown in soil-filled rhizotrons. *Funct.*
573 *Plant Biol.* **39**, 891–904 (2012).

574 2. Araus, L. & Cairns, J. E. Field high-throughput phenotyping: the new crop breeding frontier.
575 *Trends Plant Sci.* **19**, 52–61 (2014).

576 3. Montes, J. M. *et al.* Near-infrared spectroscopy on combine harvesters to measure maize
577 grain dry matter content and quality parameters. *Plant Breed.* **125**, 591–595 (2006).

578 4. White, J. W. *et al.* Field Crops Research Field-based phenomics for plant genetics research.
579 *F. Crop. Res.* **133**, 101–112 (2012).

580 5. Ferrio, J. P. *et al.* Assessment of durum wheat yield using visible and near-infrared
581 reflectance spectra of canopies. *F. Crop. Res.* **94**, 126–148 (2005).

582 6. Spielbauer, G. *et al.* High-throughput near-infrared reflectance spectroscopy for predicting
583 quantitative and qualitative composition phenotypes of individual maize kernels. *Cereal*
584 *Chem.* **86**, 556–564 (2009).

585 7. Garriga, M. *et al.* Assessing wheat traits by spectral reflectance: do we really need to focus
586 on predicted trait-values or directly identify the elite genotypes group? *Front. Plant Sci.* **8**,
587 1–12 (2017).

588 8. Weber, V. S. *et al.* Prediction of grain yield using reflectance spectra of canopy and leaves
589 in maize plants grown under different water regimes. *F. Crop. Res.* **128**, 82–90 (2012).

590 9. Aguate, F. M. *et al.* Use of hyperspectral image data outperforms vegetation indices in
591 prediction of maize yield. *Crop Sci.* **57**, 2517–2524 (2017).

592 10. Garnsworthy, P. C., Wiseman, J. & Fegeros, K. Prediction of chemical, nutritive and
593 agronomic characteristics of wheat by near infrared spectroscopy. *J. Agric. Sci.* **135**, 409–
594 417 (2000).

595 11. Oblath, E. A. *et al.* Development of near-infrared spectroscopy calibrations to measure
596 quality characteristics in intact Brassicaceae germplasm. *Ind. Crop. Prod.* **89**, 52–58 (2016).

597 12. Smith, H. F. A discrimant function for plant selection. *Ann. Eugen.* **7**, 240–250 (1936).

598 13. Hazel, L. N. The genetic basis for constructing selection indexes. *Genetics* **28**, 476–490
599 (1943).

600 14. Hastie, T., Tibshirani, R. & Friedman, J. H. *The elements of statistical learning: data mining,*
601 *inference, and prediction*. (Springer, 2009).

602 15. Bulmer, M. G. *The mathematical theory of quantitative genetics*. (Oxford University Press,
603 1985).

604 16. Falconer, D. S. & Mackay, T. F. C. *Introduction to quantitative genetics*. (Prentice Hall,
605 1996).

606 17. Fu, W. J. Penalized regressions: the Bridge versus the LASSO. *J. Comput. Graph. Stat.* **7**,
607 397–416 (1998).

608 18. Zou, H. & Hastie, T. Regularization and variable selection via the elastic net. *J. R. Stat. Soc.*
609 *B* **67**, 301–320 (2005).

19. Tibshirani, R. Regression shrinkage and selection via the LASSO. *J. R. Stat. Soc. B* **58**, 267–288 (1996).

20. Friedman, J., Hastie, T., Höfling, H. & Tibshirani, R. Pathwise coordinate optimization. *Ann. Appl. Stat.* **1**, 302–332 (2007).

21. Efron, B., Hastie, T., Johnstone, I. & Tibshirani, R. Least angle regression. *Ann. Stat.* **32**, 407–499 (2004).

22. Tattaris, M., Reynolds, M. P. & Chapman, S. C. A direct comparison of remote sensing approaches for high-throughput phenotyping in plant breeding. *Front. Plant Sci.* **7**, 1–9 (2016).

23. Babar, M. A. *et al.* Spectral reflectance to estimate genetic variation for in-season biomass, leaf chlorophyll, and canopy temperature in wheat. *Crop Sci.* **46**, 1046–1057 (2006).

24. Haboudane, D., Miller, J. R., Tremblay, N., Zarco-Tejada, P. J. & Dextraze, L. Integrated narrow-band vegetation indices for prediction of crop chlorophyll content for application to precision agriculture. *Remote Sens. Environ.* **81**, 416–426 (2002).

25. Tucker, C. J. Red and photographic infrared linear combinations for monitoring vegetation. *Remote Sens. Environ.* **8**, 127–150 (1979).

26. Gitelson, A. A., Kaufman, Y. J. & Merzlyak, M. N. Use of a green channel in remote sensing of global vegetation from EOS-MODIS. *Remote Sens. Environ.* **58**, 289–298 (1996).

27. Henderson, C. R. & Quaas, R. L. Multiple trait evaluation using relatives' records. *J. Anim. Sci.* **43**, 1188–1197 (1976).

28. Meuwissen, T. H. E., Hayes, B. J. & Goddard, M. E. Prediction of total genetic value using genome-wide dense marker maps. *Genetics* **157**, 1819–1829 (2001).

29. Soyeurt, H., Misztal, I. & Gengler, N. Genetic variability of milk components based on mid-infrared spectral data. *J. Dairy Sci.* **93**, 1722–8 (2010).

30. Dagnachew, B. S., Meuwissen, T. H. E. & Ådnøy, T. Genetic components of milk Fourier-transform infrared spectra used to predict breeding values for milk composition and quality traits in dairy goats. *J. Dairy Sci.* **96**, 5933–5942 (2013).

31. Lush, J. L. *Animal breeding plans*. (Iowa State College, Ames, 1937).

32. Friedman, J., Hastie, T. & Tibshirani, R. Regularization paths for generalized linear models via coordinate descent. *J. Stat. Softw.* **33**, 1–22 (2010).

33. Ferragina, A., de los Campos, G., Vazquez, A. I., Cecchinato, A. & Bittante, G. Bayesian regression models outperform partial least squares methods for predicting milk components and technological properties using infrared spectral data. *J. Dairy Sci.* **98**, 8133–8151 (2015).

34. R Core Team. R: A Language and Environment for Statistical Computing. (2018).

35. Bates, D., Mächler, M., Bolker, B. M. & Walker, S. C. Fitting linear mixed-effects models using lme4. *J. Stat. Softw.* **67**, 1–48 (2015).

36. Hastie, T. & Efron, B. lars: least angle regression, Lasso and forward stagewise. (2013).

Acknowledgments

We acknowledge CIMMYT's Global Wheat Program that provided both experimental field and HTP data used in this work. M.L.C. was supported by the Monsanto's Beachell-Borlaug International Scholarship Program (MBBISP).

Author contributions

R.S., S.D., J.C. and S.M. were involved in the design of the field experiments and data collection. S.M. performed the HTP data correction and georeferencing. M.L.C. and G.D.L.C. conceived the idea, performed the analyses and produced a first draft. All the authors contributed to the final manuscript.

Competing interests

The authors declare no competing interests.